IUBAT Review—A Multidisciplinary Academic Journal, 9(1): 26-48
https://doi.org/10.3329/iubatr.v9i1.91390

Numerical Simulation of MHD Mixed Convection and Heat Transfer in a Lid-Driven Hexagonal Enclosure with a Heated Wavy Cylinder

Torikul Islam[1*], Sadia Islam Rukaiya[1]

[1]*Department of Quantitative Sciences (Mathematics), IUBAT – International University of Business Agriculture and Technology, Dhaka 1230, Bangladesh*

Keywords:

FEM; Hexagonal cavity; Lid-driven; MHD; Mixed convective.

Abstract

This study investigates magnetohydrodynamic (MHD) mixed convection flow in a lid-driven hexagonal cavity containing an inner heated wavy cylinder. The flow is assumed to be time-independent, laminar, and incompressible. The upper wall moves at constant velocity and is thermally insulated, while the inner cylinder is kept at high temperature and the outer walls are cold. The governing equations are nondimensionalized and solved using the finite element method with a Galerkin formulation in COMSOL Multiphysics, and the results are validated against benchmark solutions using streamlines and isotherms. Unlike conventional cavity configurations, the presence of a wavy heated cylinder significantly modifies both vortex dynamics and thermal transport. The results demonstrate that the wavy surface enhances localized thermal intensification and promotes the formation of asymmetric secondary vortices, which are strongly governed by the combined effects of Reynolds number (Re), Richardson number (Ri), and magnetic parameter (M). The interaction between lid-driven shear flow and buoyancy-driven convection induces a non-uniform redistribution of vortical structures, with more pronounced asymmetry in secondary vortices observed at higher Ri. The findings offer essential insights into the coupled thermo-fluid-magnetic interactions within this complex geometry, providing important guidance for the development of advanced thermal systems such as MHD-based heat transfer devices.

1. Introduction

Research on mixed convection flow in lid-driven cavities has attracted significant attention due to its fundamental complexity and wide engineering applications. Mixed convection arises from the combined effects of shear-driven motion and buoyancy forces of comparable magnitudes, resulting in highly intricate flow and heat transfer characteristics. Unlike purely natural or forced convection, mixed convection represents a more realistic model for many industrial and environmental processes where thermal gradients and mechanical motions coexist. Such systems are commonly encountered in numerous industries, including heat exchangers, nuclear reactors, petroleum extraction, electronic cooling, lubrication systems, food

*Corresponding author's E-mail address: torikul.math@iubat.edu
Article received: Revised and accepted: Published:

processing, and material manufacturing processes. The lid-driven cavity system, with its simple geometry, yet exhibits highly complex fluid behavior, serves as an ideal model for exploring these phenomena. Recent studies continue to highlight these complexities across different cavity geometries and conditions. Louaraychi & Lamsaadi (2024) developed analytical and numerical correlations for mixed convection in a double lid-driven rectangular cavity with non-Newtonian fluids, showing that the effective mixed convection parameter depends strongly on the fluid's shear-thinning or shear-thickening behavior. Mansour & Jmai (2024) performed direct numerical simulations in a cubical lid-driven cavity and demonstrated how increasing Reynolds number beyond a threshold induces instability and bifurcation in the flow. Extending this to six-sided geometries, Tulu, Hirpho and Sohail (2024) investigated mixed convection with viscous dissipation in a lid-driven hexagonal cavity, revealing that the Eckert number significantly modifies thermal fields and local Nusselt distributions. Further advances include the work of Yaseen, Majeed, Ahmed and Ismael (2025b), who studied triangular lid-driven cavities with porous wavy cylinders, and found that cylinder waviness and porosity enhance the average Nusselt number, particularly at higher Darcy numbers. Bhattacharya & Basak (2025) analyzed trapezoidal cavities with moving lids and showed that multiple steady states can coexist in both natural- and mixed-convection regimes depending on Reynolds and Prandtl numbers, leading to rich bifurcation structures. Fardin, Hossain and Hasan (2025) proposed a CFD-assisted neural network framework for square lid-driven cavities with a conductive cylinder, and highlighted that the ANN reduced computational time by 82% while accurately predicting Nusselt correlations. Finally, Reddy & Srinivasan (2025) optimized mixed convection in square cavities with nanoparticle suspensions and various block orientations, finding that vertical configurations produce higher Nusselt numbers under strong buoyancy-shear interaction.

The analysis of heat transfer in lid-driven cavities has emerged as a canonical model for studying transport phenomena in confined domains where boundary motion and thermal gradients act simultaneously. Beyond their academic relevance, such systems mirror many practical processes, including drying technologies, glass melting, thermal insulation design, and chemical reactors. Structural variations such as cavity shape, internal heated inserts, or wall waviness have proven effective strategies for intensifying the flow complexity and overall thermal performance. Recent works demonstrate the diversity of approaches for enhancing heat transfer in such enclosures. Ziaur, Azad and Rahman (2024) analyzed a square cavity with a heated star-shaped obstacle filled with hybrid nanofluid and showed that the average heat transfer rate rises with Reynolds number, Richardson number, and nanoparticle fraction, while it decreases with Hartmann number, leading to nearly 50% heat transfer enhancement at higher nanoparticle loadings. Hussein, Hassan and Hameed (2024) investigated a wavy-wall cavity containing a triangular block and partial porous layers saturated by Cu-H_2O nanofluid, demonstrating that wall waviness and nanoparticle loading synergistically disrupt boundary layers and yield stronger convective heat transfer. Borahel, Zinani, Isoldi, Santos and Rocha (2025) used constructal design methods to optimize cavities with internal isothermal blocks, concluding that horizontally elongated enclosures with centrally placed blocks maximize the dimensionless heat transfer rate. Sudirman & Kamardan (2025) extended this investigation to an L-shaped cavity, showing that strong lid-induced recirculation dominates heat transfer in the upper region, while buoyancy-driven flow in the lower region promotes curved isotherms and intensified bottom-wall heat transfer. Hossain *et al.* (2025) explored a double lid-driven zigzag cavity with and without heated circular obstacles, and showed that adding circular inserts can nearly double the average Nusselt number, with nanofluid concentration further boosting thermal efficiency compared to obstacle-free cases. Finally, Alhushaybari *et al.* (2025) analyzed Casson fluid flow in a wavy-walled lid-driven cavity with diamond-shaped obstacles, reporting that higher Reynolds numbers noticeably intensify convective heat transfer in Casson fluids.

Magnetohydrodynamic (MHD) flows play a critical role in systems where electrically conducting fluids are exposed to an external magnetic field. The incorporation of MHD into mixed convection studies of lid-driven cavities has opened new pathways for actively controlling flow and heat transfer in electrically conducting fluids. By altering vortex strength, suppressing oscillations, and redistributing isotherms, magnetic fields act as non-invasive controllers of fluid motion. Such control is central to many advanced applications, including electromagnetic pumping of molten metals, desalination systems involving magnetized brine flows, thermal conditioning of plasma-facing components in fusion reactors, and magnetic cooling technologies using conductive nanofluids. Numerous investigations have explored various aspects of MHD mixed convection in enclosures with diverse geometries and boundary conditions. For instance, Shahzad, Li, Tang and Kanwal (2024) examined a hexagonal enclosure with a square obstacle under the combined effects of micro-rotation, Joule heating, porosity, and Lorentz forces, and found that the. Darcy number and micropolar effects strongly governed heat and solutal transport. Ali, S. Islam, Alim, Biplob and Z. Islam (2024) demonstrated that the hybrid nanofluid Cu-TiO2-H2O in an octagonal heat exchanger improved thermal capacity by 25.75%, although increasing Hartmann number suppressed heat transfer. Turabi & Munir (2024) investigated Casson fluid in a square cavity with an inner cylinder under inclined magnetic fields, highlighting strong sensitivity of kinetic energy and local Nusselt number to Hartmann and Casson parameters. Akter, Parveen, Munshi and Islam (2024) modeled MHD mixed convection nanofluid flow in a trapezoidal cavity with heated obstacles, concluding that nanoparticle and Darcy number substantially enhance thermal transport. Alomari *et al.* (2024) studied a split lid-driven cavity with porous blocks under magnetic influence using nanofluid, and revealed that heat transfer increased with Reynolds and Richardson numbers but decreased as Hartmann number rose. Selimefendigil & Oztop (2024) assessed hybrid nanofluid convection in a cavity with a rotating partition under magnetic fields, showing that partition size significantly influences streamlines and heat transfer, whereas stronger magnetic fields generally reduced Nusselt number. Patel, Kumar and Bagai (2024) investigated a four-sided lid-driven square cavity with sinusoidal heating, and highlighted that increasing Hartmann number dampens flow motion, leading to reduced average Nusselt number, whereas magnetic strength decreases average Sherwood number. In another study, Suma, Billah, Khan and Hoque (2025) analyzed a rectangular lid-driven cavity with a circular hollow cylinder, reporting that graphene-water nanofluid yielded the highest heat transfer as Richardson number increased, while higher Hartmann number reduced it. Souayeh (2025) examined entropy generation in a double lid-driven cavity with ternary nanofluids, highlighting that entropy generation and heat transfer both decreased under higher Hartmann numbers due to Lorentz damping. Ullah *et al.* (2025) focused on Bingham fluids in square cavities with wavy cylinders under inclined magnetic fields, showing that increasing Reynolds and Richardson numbers boosted Nusselt number, whereas higher Bingham numbers suppressed kinetic energy. Finally, Mohsin, Mahmood and Chowdhury (2025) explored hexagonal cavities with rotating cylinders and Joule heating under the influence of magnetic fields, reporting that flow modulation achieved up to 137% enhancement in thermal performance, although strong magnetic fields stabilized the flow while reducing heat transfer.

Despite the significant contributions of previous studies, several critical gaps remain. Most existing investigations are confined to canonical geometries such as square, rectangular, and circular enclosures, which do not adequately capture the complexity of practical fluid flow and heat transfer systems. In particular, the combined influence of a lid-driven hexagonal cavity containing an internal heated wavy cylinder-relevant to advanced thermal applications such as compact heat exchangers, electronic cooling systems, and solar collectors—has not yet been systematically explored. In addition, the coupled influence of complex geometries with internal wavy structures and an externally applied magnetic field under mixed convection remains insufficiently understood, highlighting a clear research gap, especially in terms of their impact on flow structure, vortex dynamics, and heat transfer performance. To address these limitations, the present study proposes a novel configuration consisting of a lid-driven hexagonal cavity with an internally heated wavy cylinder subjected to a transverse magnetic field. This configuration enables a more realistic representation of practical thermal systems while allowing a detailed examination of MHD mixed convection phenomena in geometrically complex domains. This work aims to extend the current understanding by examining the influence of Lorentz forces on flow circulation patterns and thermal transport mechanisms, and by providing a comprehensive parametric characterization of mixed convective MHD heat transfer in a geometrically complex domain. Accordingly, the specific objectives of this research are to systematically investigate the effects of key governing parameters such as *Hartmann number (Ha)*, *Reynolds number (Re)*, and *Richardson number (Ri)*, on the flow and thermal fields; to quantify the variation of the average Nusselt number with respect to these parameters; and to identify the resulting flow regimes and heat transfer characteristics within the considered configuration.

2. Mathematical Model

The study investigates a 2D, steady, laminar, incompressible mixed convective flow inside a lid-driven hexagonal cavity with an inner wavy cylinder. The schematic diagram of the physical configuration of the present problem is illustrated in Figure 1. The hexagonal enclosure, with height H, length L, and equal sides of 5 units, is considered thermally and mass insulated. The top horizontal wall moves with a uniform lid velocity U_0, while all other walls remain stationary. Gravity *g* acts in the negative *y*-direction, and a uniform magnetic strength B_0 is applied along to x-direction. The inner cylindrical wall is maintained at a constant hot temperature ($T=T_h$), the moving lid is adiabatic, and the remaining surrounding walls are kept at a cold temperature ($T=T_c$). The problem combines lid-driven forced convection, buoyancy-driven natural convection, and magnetic influences, offering insights into complicated heat transport and fluid dynamics in structured enclosures.

The coordinates of the hexagonal vertices and inner cylinder centre are provided in Table 1, labelled as: A (x_1, y_1), B (x_2, y_2), C (x_3, y_3), D (x_4, y_4), E (x_5, y_5), F (x_6, y_6), and G (x_7, y_7).

Table 1: Coordinates of the hexagonal vertices and inner cylinder centre.

1. A (x_1, y_1) = A (-0.25, 0)
2. B (x_2, y_2) = B (0.25, 0)
3. C (x_3, y_3) = C (0.5, 0.4330)
4. D (x_4, y_4) = D (0.25, 0.8660)
5. E (x_5, y_5) = E (-0.25, 0.8660)
6. F (x_6, y_6) = F (-0.5, 0.4330)
7. G (x_7, y_7) = G (0, 0.43)

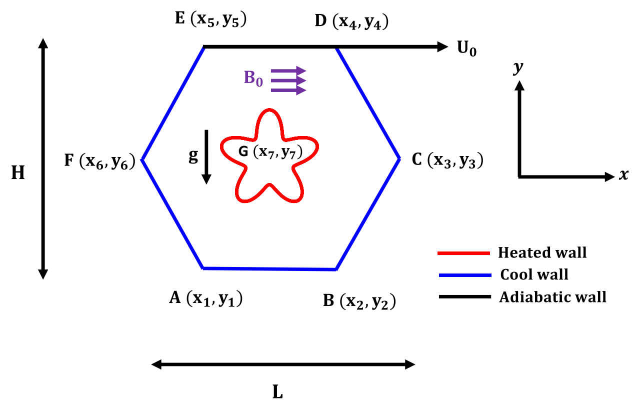

Figure 1: Schematic of the computational domain and physical configuration.

The geometry of the inner wavy cylinder is defined by:

$$\left.\begin{array}{l} r_1(\eta) = [r_0 + A\cos(2\pi N\eta)]\sin(2\pi\eta) \\ r_2(\eta) = [r_0 + A\cos(2\pi N\eta)]\cos(2\pi\eta) \end{array}\right\} \quad (1)$$

where r_0 denotes the radius of the wavy cylinder, η denotes the coordinate parameter, A is the wave's amplitude, and N represents the number of waves. In the present study, the parameters are set as $N=5$, $r_0=0.15$, and $A=0.05$.

The governing equations for mass, momentum, and energy conservation in this 2D steady mixed convective flow are expressed as, Islam, Alam, Asjad, Parveen and Chu (2021), Tulu, Hirpho and Sohail (2024b)

$$\left.\begin{array}{c} \frac{\partial u}{\partial x} + \frac{\partial v}{\partial y} = 0 \\ u\frac{\partial u}{\partial x} + v\frac{\partial u}{\partial y} = -\frac{1}{\rho}\frac{\partial p}{\partial x} + \nu\left(\frac{\partial^2 u}{\partial x^2} + \frac{\partial^2 u}{\partial y^2}\right) \\ u\frac{\partial v}{\partial x} + v\frac{\partial v}{\partial y} = -\frac{1}{\rho}\frac{\partial p}{\partial y} + \nu\left(\frac{\partial^2 v}{\partial x^2} + \frac{\partial^2 v}{\partial y^2}\right) + g\beta(T - T_C) - \frac{\sigma B_0^2}{\rho}v \\ u\frac{\partial T}{\partial x} + v\frac{\partial T}{\partial y} = \alpha\left(\frac{\partial^2 T}{\partial x^2} + \frac{\partial^2 T}{\partial y^2}\right) \end{array}\right\} \quad (2)$$

where u and v are velocity components, p is pressure, T is temperature, ν is kinematic viscosity, β is thermal expansion coefficient, σ is electrical conductivity, and α is thermal diffusivity.

The boundary conditions are:

$$\left.\begin{array}{l} \text{On the left edge}: \ u = 0, v = 0, T = T_c \\ \text{On the right edge}: u = 0, v = 0, T = T_c \\ \text{On the top horizontal wall}: u = U_0, v = 0, \frac{\partial T}{\partial y} = 0 \\ \text{On the horizontal bottom wall}: \ u = 0, v = 0, \frac{\partial T}{\partial y} = 0 \\ \text{On the surface of inner cylinder}: u = 0, v = 0, T = T_h \end{array}\right\} \quad (3)$$

To nondimensionalize Eq. (2) together with boundary conditions (3), the following dimensionless variables are introduced,

$$X = \frac{x}{L}, Y = \frac{y}{L}, U = \frac{u}{U_0}, V = \frac{v}{U_0}, P = \frac{p}{\rho U_0^2}, \theta = \frac{T - T_c}{T_h - T_c} \quad (4)$$

Substituting **Eq. (4)** into **Eq. (2)** yields the nondimensional governing equations:

$$\left.\begin{array}{c}\frac{\partial U}{\partial X}+\frac{\partial V}{\partial Y}=0\\ U\frac{\partial U}{\partial X}+V\frac{\partial U}{\partial Y}=-\frac{\partial P}{\partial X}+\frac{1}{Re}\left(\frac{\partial^2 U}{\partial X^2}+\frac{\partial^2 U}{\partial X^2}\right)\\ U\frac{\partial v}{\partial X}+V\frac{\partial V}{\partial Y}=-\frac{\partial P}{\partial Y}+\frac{1}{Re}\left(\frac{\partial^2 V}{\partial X^2}+\frac{\partial^2 V}{\partial Y^2}\right)+Ri\theta-\frac{Ha^2}{Re}\,V\\ U\frac{\partial \theta}{\partial X}+V\frac{\partial \theta}{\partial Y}=\frac{1}{RePr}\left(\frac{\partial^2 \theta}{\partial X^2}+\frac{\partial^2 \theta}{\partial Y^2}\right)\end{array}\right\} \quad (5)$$

The corresponding dimensionless boundary conditions become:

$$\left.\begin{array}{l}\text{On the left edge}: U=0, V=0, \theta=0\\ \text{On the right edge}: U=0, V=0, \theta=0\\ \text{On the top horizontal wall}: U=1, V=0, \frac{\partial \theta}{\partial Y}=0\\ \text{On the horizontal bottom wall}: U=0, V=0, \frac{\partial \theta}{\partial Y}=0\\ \text{On the surface of inner cylinder}: U=0, V=0, \theta=1\end{array}\right\} \quad (6)$$

The dimensionless parameters are defined as:

$$Ha=B_0L\sqrt{\frac{\sigma}{\mu}},\ Pr=\frac{\mu C_p}{k},\ Gr=\frac{g\beta(\mathrm{T_h}-T_c)L^3}{\nu^2},\ Re=\frac{U_0L}{\nu},\ Ri=\frac{Gr}{Re^2}$$

where, *Ha* denotes Hartmann number, *Pr* Prandtl number, *Gr* Grashof number, *Re* Reynolds number, and *Ri* the Richardson number.

The average Nusselt number on the surface of an inner heated wavy cylinder is mathematically expressed as:

$$Nu_{avg}=\frac{1}{L}\int_0^1\sqrt{\left[\left(\frac{\partial \theta}{\partial X}\right)^2+\left(\frac{\partial \theta}{\partial Y}\right)^2\right]}\,ds \quad (7)$$

where *S* denotes the surface area of the heated wall.

The streamline function ψ follows the sign convention where ψ > 0 indicates anticlockwise rotation and ψ < 0 denotes clockwise rotation. A no-slip condition is imposed along all walls. The governing vorticity–stream function relation is expressed as:

$$\frac{\partial^2 \psi}{\partial^2 \mathrm{X}}+\frac{\partial^2 \psi}{\partial^2 \mathrm{Y}}=-\left(\frac{\partial V}{\partial X}-\frac{\partial U}{\partial Y}\right)=-\Omega \quad (8)$$

where U and V denote the velocity components in the x-axis and y-axis, respectively, and Ω represents the vorticity.

3. Computational Methodology

3.1 Numerical Scheme

The nonlinear couple of PDEs (5) along with boundary conditions (6) are solved using the Galerkin Weighted Residual–Finite Element Method (GWR-FEM). The computational domain was discretized using a non-uniform unstructured triangular mesh consisting of 22444 domain elements and 872 boundary elements, well-suited to capturing the complex geometry of the hexagonal enclosure with an internal wavy cylinder. To enhance numerical accuracy, six-node quadratic triangular elements are employed. Temperature and velocity are defined at all nodes, while pressure is specified only at the corner nodes. To accurately resolve the hydrodynamic and thermal boundary layers, local mesh refinement and boundary-layer meshing are applied along the moving lid, cold walls, and heated wavy cylinder. The boundary-layer mesh consists of 8 layers with a first-layer thickness of 0.00103 and a stretching factor (growth rate) of 1.2, ensuring adequate near-wall resolution of velocity and temperature gradients. The near-wall mesh parameters were selected through successive mesh-refinement studies to ensure adequate resolution of velocity and temperature gradients. Mesh quality was evaluated using the skewness criterion available in COMSOL Multiphysics. The generated mesh exhibited a minimum element quality of 0.2305 and an average element quality of 0.7929, indicating satisfactory element quality and numerical stability for the finite-element simulations.

The GWR-FEM transforms the governing PDEs into a system of nonlinear integral equations, which are evaluated numerically using Gauss quadrature. The boundary conditions are subsequently applied to derive a simplified system of nonlinear algebraic equations. The resultant global nonlinear system is resolved iteratively employing the Newton-Raphson approach, with convergence considered achieved when the absolute error between successive iterations satisfies

$$|M^{i+1}-M^{i}|\leq 10^{-6},$$

where M represents the dependent variables (U, V, θ) and i signifies the iteration index.

The simulations are performed under steady, incompressible laminar flow conditions. To utilize the nonlinear system, a segregated iterative solver is adopted to ensure numerical stability and computational efficiency. All computations are carried out on an **Intel Core i5, 8GB RAM HP workstation** to ensure computational efficiency.

Table 2: Grid independence analysis of the present study demonstrating the variation of average Nusselt number and computational time with different mesh elements.

Elements	2142	3352	4292	6334	10628	23386	27744
Nu_{av}	6.2619	6.1164	6.0490	6.0034	5.9230	5.8999	5.8995
Computational Time	4s	4s	5s	6s	8s	17s	19s

3.2 Grid Sensitivity Analysis

A grid sensitivity analysis was carried out to ascertain the optimal number of elements in order to verify the accuracy of the current simulation for the finite element scheme using the parameters $Re = 100$, $Ri = 0.1$, $Pr = 6.9$, and $Ha = 10$. Seven nonuniform grid systems were tested with element counts of 2142 (Coarser), 3352 (Coarse), 4292 (Normal), 6334 (Fine), 10628 (Finer), 23386 (Extra Fine), and 27744 (Extremely Fine). The inner cylinder's heated, wavy wall's average Nusselt number Nu_{avg} , along with the corresponding computational times, is summarized in Table 2. As shown in Figure 2, the Nu_{avg} obtained with the 23386 elements (Extra Fine) grid is nearly identical to that of the 27744 elements (Extremely Fine) grid, indicating that the Extra Fine mesh provides sufficient accuracy while maintaining computational efficiency. Therefore, for the current exchanger fluid flow model, the domain is discretized using 23,386 triangular mesh elements. The final mesh structure is illustrated in Figure 3.

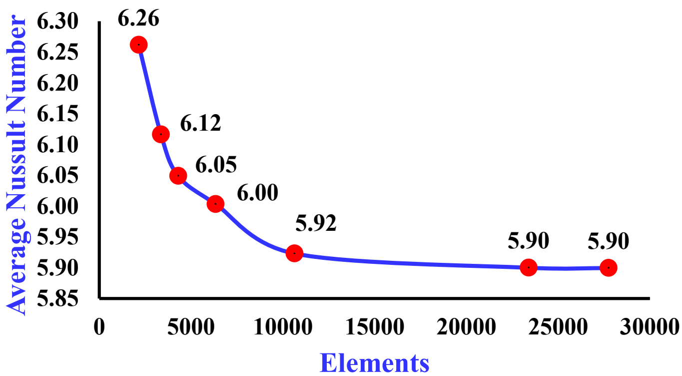

Figure 2: Sensitivity analysis of the grid based on average Nusselt number (Nuavg).

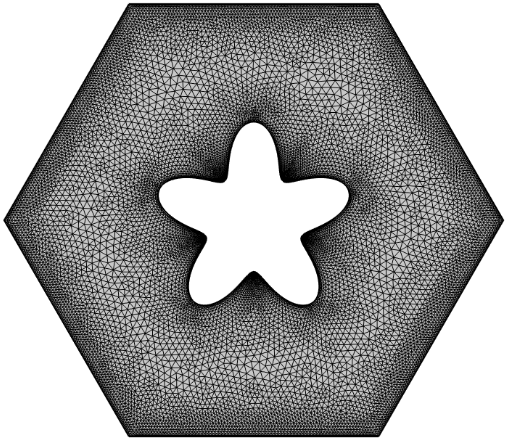

Figure 3: Mesh discretization used in the present simulation.

3.3 Code validation

To validate the numerical code of the present study, streamlines and isotherms are compared with the benchmark results of Cheng (2011) for a lid-driven square cavity, in which the upper wall moves in the positive x-direction (Figure 4). In Cheng's configuration, both vertical sidewalls are adiabatic, the bottom wall is heated, and the top wall is kept cold. The present results are further validated through comparison with the work of Tulu, Hirpho and Sohail (2024) for an upper-wall-driven hexagonal enclosure, illustred in Figure 5. The excellent agreement between the present streamlines and isotherms with the reference data strongly validates the accuracy of the numerical code and instills confidence in the subsequent findings of this investigation.

Cheng (2011)

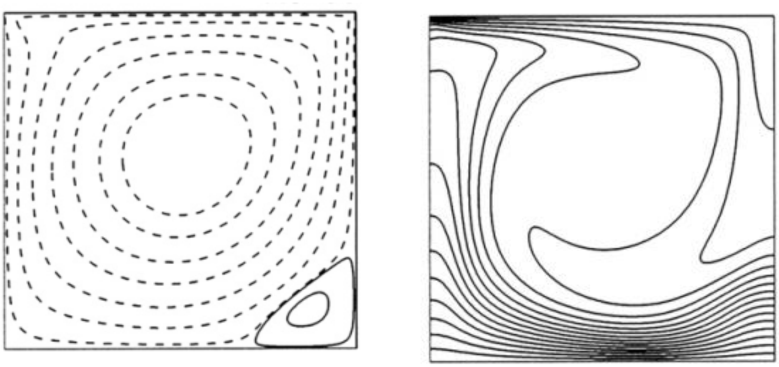

Present

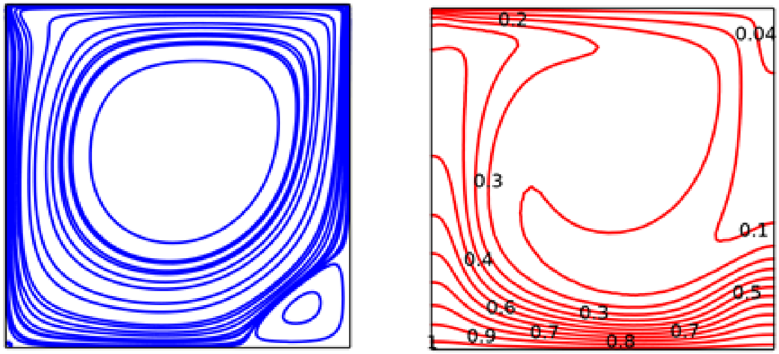

(a) Streamline **(b) Isothermal line**

Figure 4: Comparison of the present study results for Re=300, Ri=1, Ha=0, and Pr=0.71.

Tulu et al. (2024)

Present

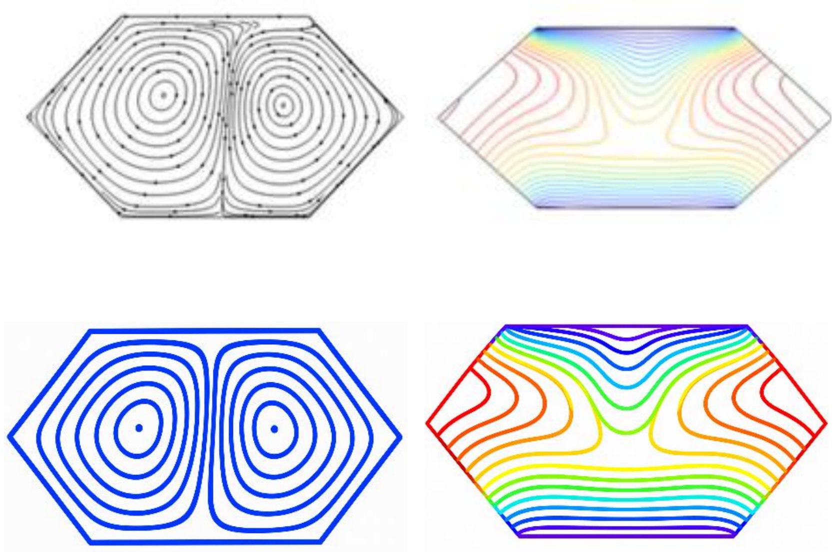

(a) Streamline **(b) Isothermal line**

Figure 5: Comparison with Tulu *et al.* (2024) for Re=100, Ri=1, Ha=0, and Pr=6.25.

4. Results and Discussions

In this section, the varying results of mixed convective MHD flow in a lid-driven hexagonal cavity with an inner wavy cylinder, simulated using the GWR-FEM, are presented. Numerical simulations are conducted for Richardson number *(Ri=0.01, 0.1, 100, 1000)*, Reynolds number *(Re=10, 100, 500, 1000)*, and Hartmann number *(Ha=10, 25, 50, 100)*. The outcomes are illustrated through streamlines, isotherm contours, and average Nusselt numbers, while the Prandtl number is fixed at Pr = 6.9.

Impact of Ri on Streamline and Isothermal lines:

The Richardson number Ri governs the relative strength of buoyancy forces to inertial forces and therefore determines the transition between forced and natural convection regimes. Figure 6 illustrates the evolution of the flow and thermal fields for Re = 100, Ha = 10, and Pr = 6.9 as Ri increases from 0.01 to 1000. At low Richardson numbers (Ri = 0.01 and 0.1), inertial forces generated by the moving lid dominate the momentum balance, producing a single large primary vortex that occupies most of the cavity. The shear layer generated beneath the lid transfers momentum efficiently into the fluid interior, while buoyancy effects remain too weak to alter the vortex structure significantly. Consequently, the hydrodynamic boundary layer along the moving wall governs the flow behavior, and the streamline distribution remains closely aligned with the lid motion. As Ri increases to 100, buoyancy forces become comparable to the lid-induced inertial forces, resulting in a mixed-convection regime. The upward motion of the heated fluid around the wavy cylinder opposes and redistributes the horizontal momentum imparted by the lid. This force competition causes deformation of the primary vortex and promotes vortex splitting into two dominant recirculating cells adjacent to the cylinder. The interaction between the thermal boundary layer surrounding the heated cylinder and the shear-driven boundary layer beneath the lid intensifies fluid mixing and generates stronger vertical transport. At Ri = 1000, buoyancy becomes the dominant driving mechanism. The heated fluid rises along the cylinder surface, while cooler fluid descends along the sidewalls, forming nearly symmetric counter-rotating vortices. The emergence of a secondary eddy beneath the cylinder reflects local flow separation induced by strong buoyancy-driven recirculation. Under these conditions, the flow structure is controlled primarily by gravitational forces rather than lid motion. The corresponding isotherm distributions further demonstrate the transition in heat-transfer mechanisms. At low Ri, the thermal field remains confined near the heated cylinder, indicating that heat transport is dominated by conduction with only limited convective redistribution. The thermal boundary layer remains relatively thick and undisturbed. As Ri increases to 100, buoyancy-induced vertical motion strengthens thermal advection, causing substantial bending of the isotherms and the formation of thermal plumes. The enhanced interaction between the velocity and thermal boundary layers reduces thermal boundary-layer thickness and increases heat-transfer effectiveness. At Ri = 1000, the isotherms become nearly vertical, indicating that heat transport is dominated by buoyancy-driven convection. The strong upward movement of hot fluid and downward movement of cold fluid establish an efficient circulation loop that suppresses conductive dominance and significantly enhances convective heat transport throughout the enclosure.

Impact of Re on Streamline and Isothermal lines:

Figure 7 depicts the influence of the Reynolds number on the flow and thermal structures for Ri = 0.1, Ha = 10, and Pr = 6.9. Since Reynolds number represents the ratio of inertial to viscous forces, increasing Re strengthens momentum transport while reducing the relative damping effect of viscosity. At Re = 10, viscous forces dominate the flow field, producing a broad and weak recirculation zone beneath the moving lid. Momentum diffusion is significant, resulting in a thick hydrodynamic boundary layer and relatively weak circulation around the heated cylinder. As Re increases from 100 to 1000, inertial effects become increasingly dominant, enhancing the penetration of lid-driven momentum into the cavity. The primary vortex strengthens, its core shifts in the direction of lid motion, and the streamline density increases around the heated cylinder. The stronger circulation reflects a reduction in viscous dissipation and a more effective transfer of momentum from the moving wall to the fluid interior. Furthermore, the interaction between the accelerating flow and the obstacle-induced pressure gradients promotes stronger vortex stretching and recirculation around the cylinder. The progressive displacement of the vortex core toward the lower-right region of the cavity is indicative of the increasing dominance of inertial transport over viscous diffusion. The thermal field responds directly to these hydrodynamic changes. At Re = 10, heat transfer is primarily controlled by diffusion, as evidenced by the nearly concentric isotherms surrounding the heated cylinder. The relatively thick thermal boundary layer limits thermal transport into the bulk fluid. As Re increases, stronger advection transports heated fluid away from the cylinder more efficiently, resulting in greater isotherm distortion and thermal plume elongation. The enhanced shear near the heated surface continuously renews the fluid adjacent to the cylinder, thereby reducing the thermal boundary-layer thickness. At Re = 1000, vigorous circulation promotes intense fluid mixing throughout the cavity, causing substantial redistribution of thermal energy and a marked increase in convective heat-transfer efficiency. Thus, increasing Reynolds number strengthens vortex dynamics, enhances boundary-layer thinning, and promotes advection-dominated heat transfer.

Impact of Ha on Streamline and Isothermal lines:

Figure 8 illustrates the influence of the Hartmann number on the flow and thermal fields for Re = 100, Ri = 0.1, and Pr = 6.9. The Hartmann number quantifies the ratio of electromagnetic forces to viscous forces. As Ha increases, the applied magnetic field generates a Lorentz force that acts opposite to the fluid motion, producing an electromagnetic braking effect. This Lorentz-force-induced damping dissipates kinetic energy and suppresses vortex formation throughout the cavity. At Ha = 10, the Lorentz force is relatively weak compared with the inertial force generated by the moving lid. Consequently, a strong primary vortex occupies most of the enclosure, and the lid-driven shear layer effectively transfers momentum to the fluid interior. When Ha increases to 25 and 50, the Lorentz force progressively counteracts fluid motion and reduces vortex strength. The electromagnetic damping suppresses velocity fluctuations and inhibits momentum transport away from the moving wall. As a result, the vortex core shrinks and the recirculation region becomes increasingly confined to the vicinity of the lid. Simultaneously, the hydrodynamic boundary layer thickens because the magnetic field weakens the velocity gradients responsible for sustaining circulation. At Ha = 100, Lorentz-force dominance almost completely suppresses the primary vortex, leaving only a shallow recirculating layer beneath the moving wall. This behavior is characteristic of magnetohydrodynamic damping, where electromagnetic forces convert kinetic energy into Joule dissipation and significantly reduce fluid motion. The isothermal distributions exhibit corresponding changes. At low Ha, strong circulation promotes convective transport, producing distorted isotherms and a well-developed thermal plume extending from the heated cylinder. As the magnetic field strengthens, the suppression of fluid motion weakens thermal advection and reduces the interaction between the velocity and thermal boundary layers. Consequently, the thermal plume diminishes and the isotherms become progressively more concentric around the cylinder. At Ha = 50 and particularly at Ha = 100, the temperature contours approach symmetry, indicating that heat transfer occurs predominantly through conduction rather than convection. The reduction in convective transport originates directly from Lorentz-force-induced damping, which suppresses vortex motion, thickens the thermal boundary layer, and limits the ability of the flow to redistribute thermal energy throughout the cavity. Therefore, increasing Hartmann number weakens vortex dynamics and progressively shifts the heat-transfer mechanism from convection-dominated to conduction-dominated transport.

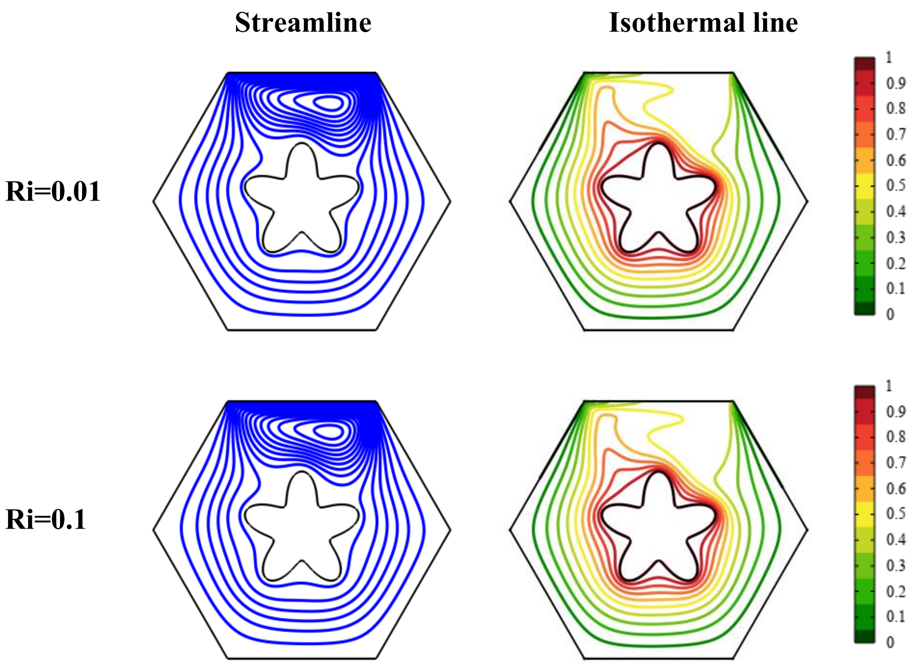

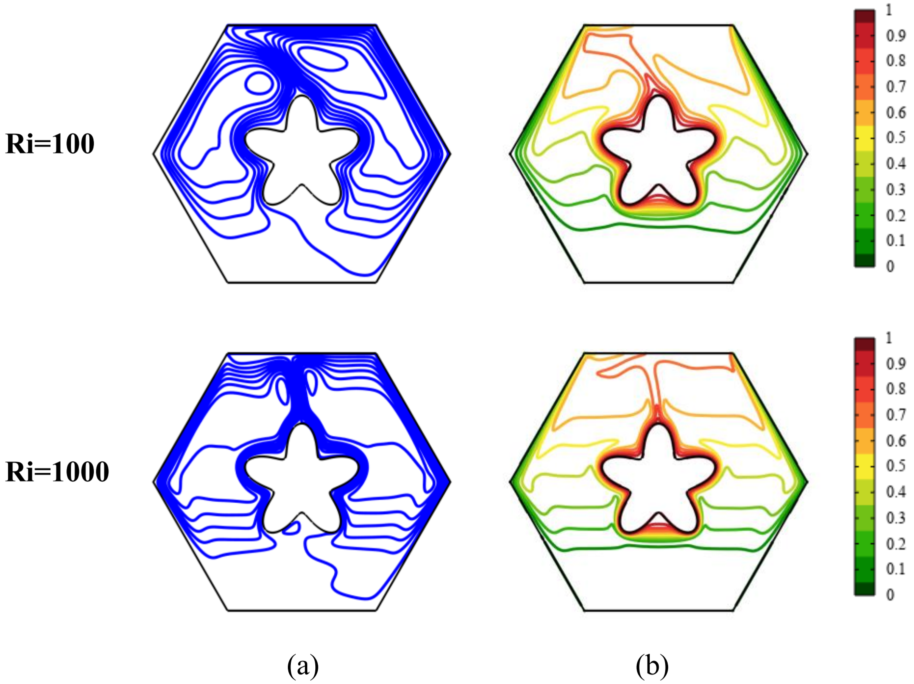

Figure 6: Impact of Ri on (a) Streamline, (b) Isothermal line for Re=100, Ha=10, Pr=6.9.

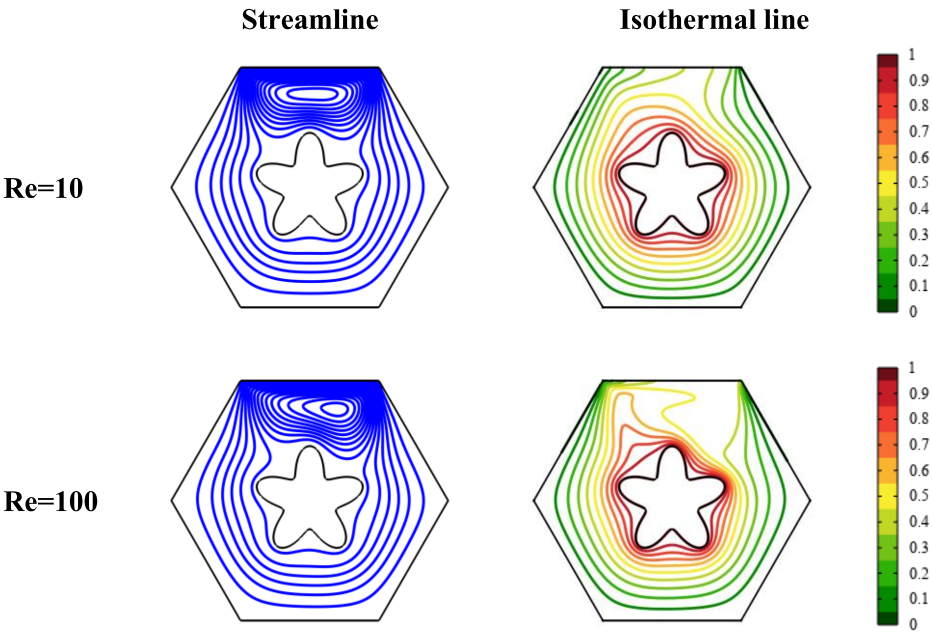

Re=500

Re=1000

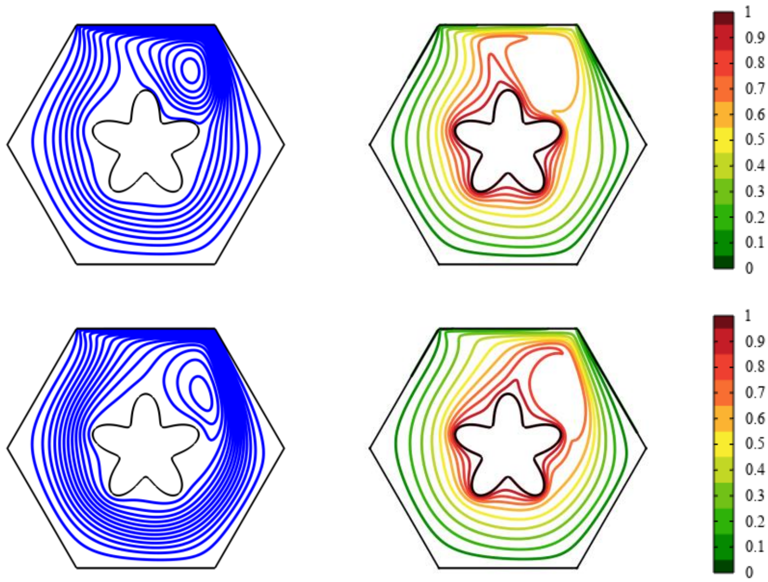

(a) **(b)**

Figure 7: Impact of Re on (a) Streamline, (b) Isothermal line for Ri=0.1, Ha=10, Pr=6.9.

Streamline **Isothermal line**

Ha=10

Ha=25

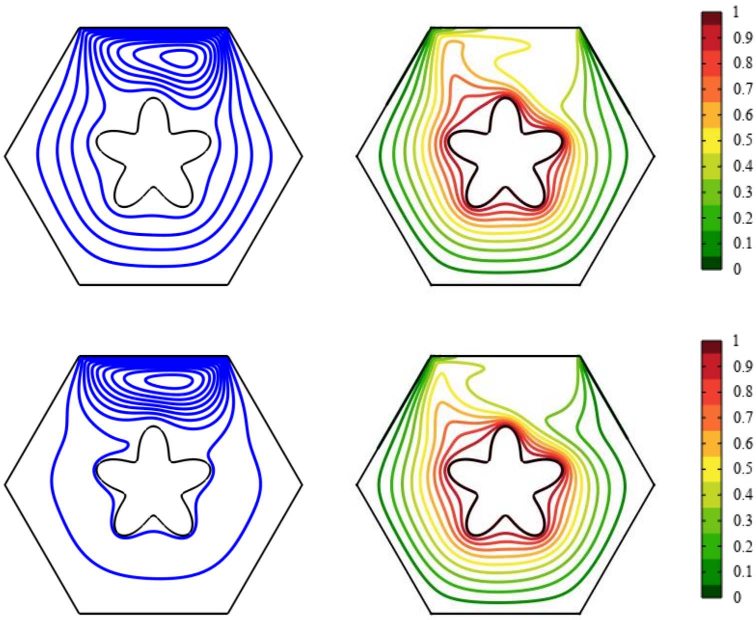

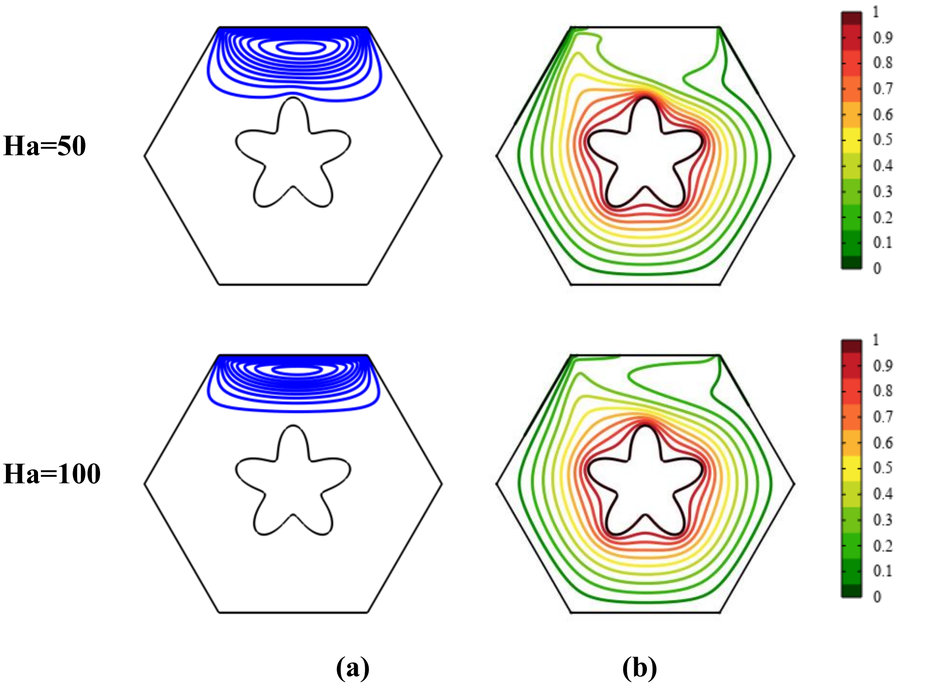

Figure 8: Impact of Ha on (a) Streamline, (b) Isothermal line for Re=100, Ri=0.1, Pr=6.9.

Impact of Ri on Heat Transfer Rate:

The variation of the average Nusselt number *(Nu_{avg})* with Richardson number *(Ri)*, presented in Figure 9, demonstrates a monotonic increase, highlighting a fundamental shift in the dominant heat transfer mechanism**.** It is observed that when Ri increases from 0.01 to 0.1, Nu_{avg} remains almost unchanged, indicating that forced convection dominates over buoyancy effects in this regime. However, as Ri increases further from 0.1 to 100, Nu_{avg} rises significantly by nearly 183%, highlighting the strong influence of natural convection in enhancing heat transfer. Beyond this range, for Ri between 100 and 1000, Nu_{avg} continues to increase but at a reduced rate of about 75%, suggesting that the system approaches a buoyancy-driven convection regime where further enhancement becomes less pronounced due to the asymptotic behavior of natural convection.

Impact of Re on Heat Transfer Rate:

The variation of the average Nusselt number *(Nu_{avg})* with Reynolds number (Re), presented in Figure 10. It shows an overall increasing trend with Re from 10 to 500, is predominantly a monotonic increase in the average Nusselt number *(Nu_{avg})* consistent with the strengthening of forced convection mechanisms. As Re increases from 10 to 100, Nu_{avg} rises by approximately 30%, and further increases to 500, Nu_{avg} rises 28%; this is attributed to the corresponding thinning of the thermal boundary layer under stronger inertial forces. However, a notable deviation occurs as Re increases from 500 to 1000, where Nu_{avg} experiences a 6% decrease. This decline is attributed to the onset of localized flow separation and intensified recirculation zones, which weaken the effective fluid–solid thermal interaction and suppress convective transport in the vicinity of the heated surface. Consequently, despite the increase in flow intensity, the heat transfer performance slightly deteriorates due to the altered flow structure and reduced near-wall mixing efficiency.

Impact of Ha on Heat Transfer Rate:

The influence of Hartmann number *(Ha)* on heat transfer is depicted in Figure 11, showing an overall decreasing trend in the average Nusselt number *(*Nu_{avg}*)* due to the magnetic field's suppressive impact on fluid motion. As Ha increases from 10 to 25, a very slight increase of approximately 0.17% in *(*Nu_{avg}*)* is observed. This marginal enhancement can be attributed to the initial action of the Lorentz force, which modifies the flow structure by reorganizing weak convective eddies, leading to a temporary improvement in local mixing before magnetic damping becomes dominant. Beyond this range, however, increases in Ha from 25 to 50 and from 50 to 100 lead to pronounced reductions in Nu_{avg} of about 7% and 10%, respectively. This reduction is due to the progressive dominance of the Lorentz force, which suppresses fluid motion, damps velocity fluctuations, thereby stabilizing the flow field. As the magnetic field strength intensifies, both forced and natural convection are increasingly suppressed, leading to a more laminarized and stagnant flow, and consequently diminishing the overall convective heat transfer performance.

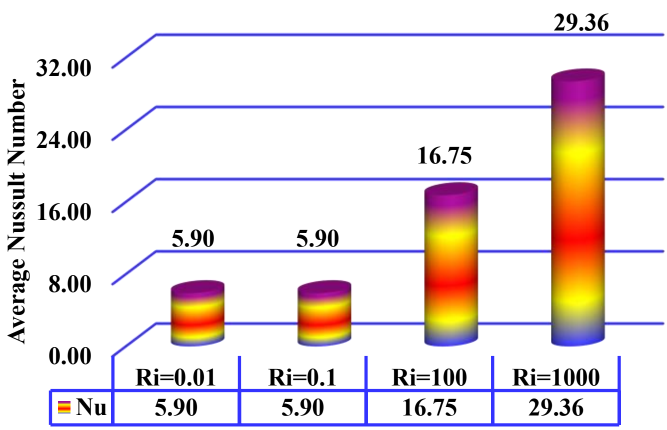

Figure 9: Effect of Ri on average Nusselt number (Nu_{avg}).

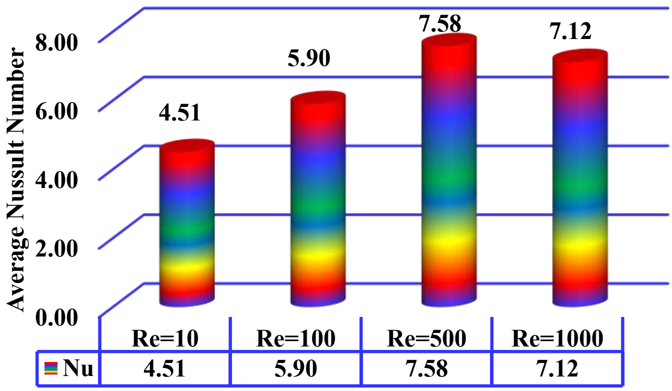

Figure 10: Effect of Re on average Nusselt number (Nu_{avg}).

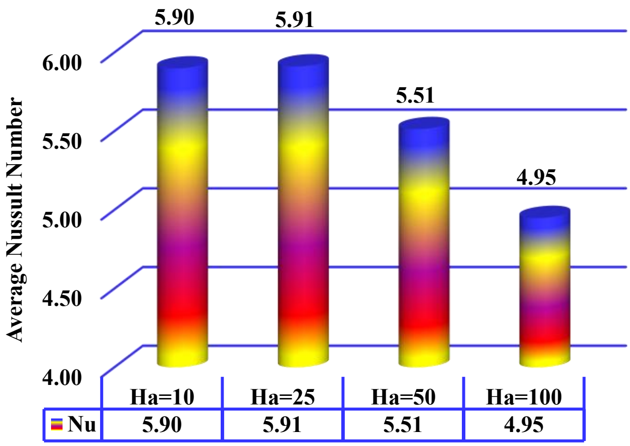

Figure 11: Effect of Ha on average Nusselt number (Nu_{avg}).

5. Conclusion

This study numerically investigates mixed convective MHD flow and heat transfer in a hexagonal cavity containing a wavy heated cylinder using the Galerkin residual-based FEM implemented in COMSOL Multiphysics. The simulations were performed on a Core i5 system with 8 GB of RAM. The effects of key physical parameters, *Richardson number (Ri)*, *Reynolds number (Re)*, and *Hartmann number (Ha)* on the thermo-fluid dynamics are thoroughly examined. These effects are quantified through the average Nusselt number and visualized via streamline patterns and isotherm distributions. The results provide critical physical insight into the heat transfer mechanisms governing such complex MHD systems. This work establishes a valuable benchmark for applications in advanced thermal management, crystal growth processes, and nuclear reactor design, where complex geometries and magnetic fields are present. The core findings of the study are listed below:

- A single dominant vortex forms in the cavity at low Richardson numbers *(Ri)*, whereas at higher *Ri* (e.g., $Ri \geq 100$), the flow transitions into a two-vortex structure.
- A substantial enhancement in Nu_{avg} of approximately **397%** occurs as *Ri* increases from 0.01 to 1000.
- A moderate increase of Nu_{avg}, approximately 57% is observed as *Reynolds number (Re)* rises from 10 to 1000.
- The magnetic field suppresses convection, leading to a 16% reduction in Nu_{avg} as *Hartmann number (Ha)* increases from 10 to 100.

Acknowledgement

The authors gratefully acknowledge the Miyan Research Institute, International University of Business Agriculture and Technology, Dhaka 1230, Bangladesh, for their valuable support and assistance.

Conflict of interest

The authors declare that there are no potential conflicts of interest regarding the publication of this work. Furthermore, the authors confirm that all ethical considerations, including plagiarism, informed consent, research misconduct, data fabrication or falsification, duplicate publication or submission, and redundancy, have been fully observed

References

Akter, H., Parveen, N., Munshi, M., & Islam, T. (2024). MHD Mixed Convection of Nanofluid in a Lid-Driven Porous Trapezoidal Cavity with a Heated Obstacle. *Multiscale Science and Engineering*, *6,* 57-77. https://doi.org/10.1007/s42493-024-00113-x

Alhushaybari, A., Khan, S. A., Farooq, U., Imran, M., Mehdi Haider, S. M., Chuan Ching, D. L., & Khan, I. (2025). Thermal management analysis of thermal radiation effect on mixed convective casson fluid inside wavy wall lid-driven cavity with diamond-shaped obstacles. *Journal of Radiation Research and Applied Sciences*, *18*(3), 101808. https://doi.org/https://doi.org/10.1016/j.jrras.2025.101808

Ali, Md. Y., Islam, S., Alim, M. A., Biplob, R. A., & Islam, Md. Z. (2024). Numerical investigation of MHD mixed convection in an octagonal heat exchanger containing hybrid nanofluid. *Heliyon*, *10*(17), e37162. https://doi.org/https://doi.org/10.1016/j.heliyon.2024.e37162

Alomari, M. A., Al-Farhany, K., Al-Salami, Q. H., Ali, I. R., Biswas, N., Mohamed, M. H., & Alqurashi, F. (2024). Numerical analysis to investigate the effect of a porous block on MHD mixed convection in a split lid-driven cavity with nanofluid. *International Journal of Thermofluids*, *22*, 100621. https://doi.org/https://doi.org/10.1016/j.ijft.2024.100621

Bhattacharya, M., & Basak, T. (2025). Multiple steady states for various regimes of convection (natural or mixed) dominance within a lid-driven trapezoidal cavity. *Physics of Fluids*, *37*(2), 23625. https://doi.org/10.1063/5.0252338

Borahel, R., Zinani, F., Isoldi, L., dos Santos, E., & Rocha, L. (2025). Analysis of the Design of Cavities with Isothermal Blocks under Mixed Convection. *Journal of Applied and Computational Mechanics*, *11*(2), 541–556. https://doi.org/10.22055/jacm.2024.47208.4676

Cheng, T. S. (2011). Characteristics of mixed convection heat transfer in a lid-driven square cavity with various Richardson and Prandtl numbers. *International Journal of Thermal Sciences*, *50*(2), 197–205. https://doi.org/https://doi.org/10.1016/j.ijthermalsci.2010.09.012

Fardin, M. M., Hossain, M. S., & Hasan, M. N. (2025). CFD based neural network model framework for mixed convection in a lid-driven cavity with conductive cylinder. *Heliyon*, *11*(4), e42637. https://doi.org/https://doi.org/10.1016/j.heliyon.2025.e42637

Hossain, Md. A., Sajib, M. A. H., Sagib, Md., Islam, Md. R., Barai, G., Podder, C., & Saha, B. K. (2025). Enhanced thermal efficiency on mixed convection flow of TiO2 – Water nanofluid inside a double lid driven zigzag cavity with and without heated obstacles insertion. *International Journal of Thermofluids*, *25*, 101040. https://doi.org/https://doi.org/10.1016/j.ijft.2024.101040

Hussein, R. A., Hassan, A. M., & Hameed, R. H. (2024). Mixed convection heat transfer in a partial porous layered split lid-driven wavy wall cavity with Cu–H2O nanofluid. *Numerical Heat Transfer, Part B: Fundamentals*, *0*(0), 1–27. https://doi.org/10.1080/10407790.2024.2343329

Islam, T., Alam, Md. N., Asjad, M. I., Parveen, N., & Chu, Y.-M. (2021). Heatline visualization of MHD natural convection heat transfer of nanofluid in a prismatic enclosure. *Scientific Reports*, *11*(1), 10972. https://doi.org/10.1038/s41598-021-89814-z

Louaraychi, A., & Lamsaadi, M. (2024). Correlations of mixed convection in a double lid-driven shallow rectangular cavity: The case of non-Newtonian power-law fluids. *Heat Transfer*, *53*(8), 4394–4421. https://doi.org/https://doi.org/10.1002/htj.23138

Mansour, N. Ben, & Jmai, R. (2024). Direct Numerical Simulation of Mixed Convection Flow in Lid-Driven Cavities. *Physical Science International Journal*, *28*(3), 50–65. https://doi.org/10.9734/psij/2024/v28i3831

Mohsin, F. T., Mahmood, F. T., & Chowdhury, T. S. (2025). Control of MHD Conjugate Mixed Convection in a hexagonal cavity with Flow Modulation and Joule heating. *ASME Journal of Heat and Mass Transfer*, 1–23. https://doi.org/10.1115/1.4069267

Patel, A., Kumar, M., & Bagai, S. (2024). Heat and mass transfer under MHD mixed convection in a four-sided lid-driven square cavity. *Heat Transfer*, *53*(3), 1220–1266. https://doi.org/https://doi.org/10.1002/htj.22993

Reddy, T. R. K., & Srinivasan, D. R. (2025). Numerical investigation of mixed convection in a square lid-driven cavity with influence of orientation and nanoparticle addition on heat transfer characteristics: Multi-objective optimization approach. *Journal of Thermal Engineering*, *11*(3), 685–702. https://izlik.org/JA75EN77DJ

Selimefendigil, F., & Oztop, H. F. (2024). Effects of a rotating partition on mixed convection of hybrid nanofluid in a lid-driven cavity under different magnetic fields. *Physics of Fluids*, *36*(1), 12013. https://doi.org/10.1063/5.0176687

Shahzad, H., Li, Z., Tang, T., & Kanwal, M. (2024). Impact of micro-rotation on a double-diffusive radiative flow within a lid-driven enclosure fearuring Joule heating, porosity and Lorentz forces. *Journal of Molecular Liquids*, *406*, 125067. https://doi.org/https://doi.org/10.1016/j.molliq.2024.125067

Souayeh, B. (2025). Numerical Analysis of Magnetohydrodynamics Mixed Convection and Entropy Generation in a Double Lid-Driven Cavity Using Ternary Hybrid Nanofluids. *Advanced Theory and Simulations*, *8*(5), 2401357. https://doi.org/https://doi.org/10.1002/adts.202401357

Sudirman, N. H., & Kamardan, M. G. (2025). A Study on Mixed Convection Heat Transfer in Lid-Driven L-Shaped Cavity using COMSOL. *Enhanced Knowledge in Sciences and Technology*, *5*(1), 32–38. https://doi.org/10.1016/j.icheatmasstransfer.2017.05.025

Suma, U. K., Billah, M. M., Khan, A. R., & Hoque, K. E. (2025). Magnetohydrodynamic mixed convective heat transfer augmentation in a rectangular lid-driven enclosure with a circular hollow cylinder utilizing nanofluids. *International Journal of Thermofluids*, *25*, 101014. https://doi.org/https://doi.org/10.1016/j.ijft.2024.101014

Tulu, A., Hirpho, M., & Sohail, M. (2024a). Modeling and simulation of mixed convection flow with viscous dissipation in a lid-driven hexagonal cavity using finite element method. *International Journal of Thermofluids*, *22*, 100702. https://doi.org/https://doi.org/10.1016/j.ijft.2024.100702

Turabi, Y. U. U. Bin, & Munir, S. (2024). CFD simulations of MHD effects on mixed convectional flow in a lid-driven square cavity with square cylinder using Casson fluid. *Numerical Heat Transfer, Part B: Fundamentals*, *86*(51), 3742-3757. https://doi.org/10.1080/10407790.2024.2365890

Ullah, I., Ullah, H., Nadeem, S., Alzabut, J., Saleem, S., & Alblawi, A. (2025). Inclined MHD mixed convection of a Bingham fluid in a lid-driven square cavity with an embedded wavy cylinder: thermal and magnetic field interactions. *Journal of Thermal Analysis and Calorimetry*, *150*, 10105-10126. https://doi.org/10.1007/s10973-025-14279-5

Yaseen, D. T., Majeed, A. J., Ahmed, S. S., & Ismael, M. A. (2025). Impact of a wavy wall triangular porous cylinder on diffusive-mixed convection in a lid-driven triangular cavity. *International Journal of Thermofluids*, *25*, 101007. https://doi.org/https://doi.org/10.1016/j.ijft.2024.101007

Ziaur, R. M., Azad, A. K., & Rahman, M. M. (2024). Sensitivity study on convective heat transfer in a driven cavity with star-shaped obstacle and hybrid nanofluid using response surface methodology. *Heliyon*, *10*(17), e37440. https://doi.org/https://doi.org/10.1016/j.heliyon.2024.e37440